INDIVIDUALIZED DIFFEOMORPHIC MAPPING FOR STROKE PATIENTS WITH LARGE CORTICAL INFARCTS

Soon Hock Wei

Department of Bioengineering

National University of Singapore

A thesis submitted for the degree of

Master of Engineering (M.Eng)

2013 JANUARY

1. Reviewer:

2. Reviewer:

Signature from head of M.Eng committee:

Abstract

Whole brain mapping for stroke patients with large cortical infarcts poses a challenge to conventional automatic whole brain mapping algorithms. These algorithms minimize a quantified measure of differences between images with a pre-determined atlas, and are commonly formulated based on parameters such as their intensity values. This causes an ensuing mismatch in the areas of signal loss, in particular, the regions containing cortical infarcted brain tissues, as they are not found in the atlas. In this study, we investigated an individualized approach of whole brain mapping for stroke patients with large cortical infarcts. We proposed a framework based on Large Deformation Diffeomorphic Metric Mapping (LDDMM) with individualized anatomical features extraction and cost function masking, for registering an atlas to a brain with large cortical infarcts. We applied this technique to 2 separate datasets (of either real or simulated cortical infarcts) of different databases and validated the mapping accuracy using selected quantitative measures. Our results revealed that our mapping technique for stroke patients produced comparable accuracy with LDDMM for healthy controls without cortical infarcts. Hence, we consider this as the preferred method of choice in brain image mapping with large cortical infarcts.

Acknowledgements

I would like express my utmost heartfelt gratitude to my advisor Dr. Qiu Anqi for her unrelenting supports and guidance throughout the whole course of my research.

Besides, I would like to thank my lab mates who have helped me in one way or another in this project. They are such a wonderful people to work with.

Last but not least, my dearest family members who have never stop believing in me.

Contents

List of Figures

List of Tables

1

Introduction

1.1 The Research Problem

Whole brain mapping (also known as brain spatial normalization, brain registration or brain alignment) is widely used in neuroimaging research to align the brains onto some common stereotactic space. This is particularly important in fMRI studies, in which the aforementioned technique is often employed to transform brains for group analysis and comparison. In the context of brains with large cortical infarcts, precise brain mapping improves the presentation and analysis of lesion locations and any associated behavioral changes (1). Nevertheless, whole brain mapping for stroke patients with large cortical infarcts poses a challenge to conventional automatic whole brain mapping algorithms. These algorithms minimize a quantified measure of differences between images with a pre-determined atlas, and are commonly formulated based on parameters such as their intensity values. This causes an ensuing mismatch in the areas of signal loss, in particular, the regions containing cortical infarcted brain tissues, as they are not found

in the atlas. This could cause the normalization algorithm to attempt further transformation in order to minimize the cost function, even in cases where optimal matching for other healthy brain tissue has already been achieved. This confounded and biased normalization usually leads to significant and inappropriate image distortion.

2

Literature Review

2.1 Whole Brain Mapping for Stroke Patients with Large Cortical Infarcts

Thus far, there are only a few available brain mapping approaches that deal with brain images with large cortical infarcts. An early solution implemented a linear affine registration which accounted only for the overall size, shape, position and orientation of the brain, resulting in poor and restricted fitting of the local structures. As detailed non-linear warping was not performed by the algorithm, distortions were not introduced in and around the infarct area. Alternatively, enantiomorphic normalization (2) essentially creates an artificial brain by replacing the lesion volume with a homologous volume from its contra-lateral hemisphere. Non-linear normalization parameters were estimated from this artificial brain and were then, applied onto the original. This method, however, is only applicable to unilateral cortical infarctions and assumes, erroneously, that

the brain is symmetrical, despite clear evidence saying otherwise (3). Ashburner, J. et al introduced an iterative unified model that combines segmentation, bias correction, and spatial normalization with the use of tissue map priors of the white matter, gray matter and cerebrospinal fluid (CSF) (4). Multiple Gaussian models for tissue segmentation distinguish infarcted and healthy brain regions, while bias correction may model the infarcted tissue as an area of inhomogeneity. Hence, spatial normalization of cortical infarcts in this approach benefits from the segmentation and bias correction in an integrative manner. Brett and colleagues (1) proposed a cost function masking (CFM) approach by masking off the lesion voxels when calculating differences between two brain images. This approach significantly improved the non-linear normalization results and outperformed non-linear normalization (without CFM) approaches in SPM99. One associated drawback, however, is the manual and laborious delineation of a lesion mask for each infarcted brain. In spite of its tediousness, CFM remains widely used. In 2010 (5), Anderson and colleagues highlighted its importance by showing that even with the use of the unified segmentation approach (4), the cost function masking remains necessary in normalizing brain images with chronic infarcts. However, both CFM and unified segmentation approaches are based on small deformation model, limiting its use for diffuse infarction pathology.

Aligning brain images with large cortical infarcts has thus far limited to volume-based nonlinear registration approaches. Such approaches seek the deformation that is driven by intensity information, and hence, provide accurate mappings in subcortical and ventricular regions where intensity contrast is clear and structural shapes are relatively simple. However, these approaches fail to accurately align the cortical region since the convoluted cortical sheet cannot be

well characterized based on image intensity alone. There is an additional need to consider the geometric property of the cortex as functionally distinct regions are close to each other in a volume space but geometrically distant in terms of distance measured along the cortex. Such a geometric property of the cortex has been well preserved in a cortical surface model (6, 7). Registration approaches based on cortical surfaces (6, 8, 9, 10) have shown superior performance in the alignment of highly complex cortical folding pattern over volume-based registration approaches, and thus resulted in increased statistical power for averaging of functional data in the cortical region across subjects (11).

Recent works by Postelnicu et al. (12) and Joshi et al. (13, 14) have employed the sphererical cortical surface mapping implemented in FreeSurfer (6) or the harmonic cortical surface mapping constrained by gyral/sulcal curves (13, 14) to first seek the deformation field on the cortical boundary and then extend it to the 3D volume for further brain volume registration. These two approaches have shown tremendous improvement in mapping accuracy when compared to the advanced volume-based approach, hierarchical attribute matching mechanism for image registration (HAMMER) (15), where geometric features of the cortex have been intrinsically incorporated. Only recently, Du et al. (16) proposed the approach providing an one-to-one, differentiable, and invertible deformation field that simultaneously aligns gyral/sulcal curves, cortical surface, and intensity image volume from one subject to the other under the framework of large deformation diffeomorphic metric mapping (LDDMM). This approach with superior mapping accuracies (for both cortical and subcortical structures) as compared to LDDMM based solely on image intensity, combined volumetric and surface registration (12) and hierarchical attribute matching mechanism for elastic reg-

istration (HAMMER) (15). Nevertheless, there is no literature evidence to show that this approach works well with brains with large cortical infarcts.

3

Aims of the project

3.1 Objectives

In this study, we aimed to register a brain atlas to brains with large cortical infarcts, and to achieve good alignment in the intact cortical and subcortical regions of the infarcted brains. Hence, we employed the whole brain LDDMM algorithm described in (16) and proposed a brain mapping framework that individualizes anatomical features, such as cortical surfaces, sulcal/gyral curves, surfaces of the lateral ventricles, and intensity images. We incorporated these individualized anatomical features into the LDDMM algorithm to 1) mask out cortical infarct regions; 2) well constrain the boundary of cortical infarcts; 3) well align anatomical features in the intact brain regions. We quantitatively validated this mapping framework in terms of gyral/sulcal curve anatomical variation, sulcal region alignment, as well as structural segmentation in both cortical and subcortical regions using brain images with simulated cortical infarcts and brain images of stroke patients.

4

Methodology

In this section, we will describe a new framework for aligning brain image of a healthy brain to a targeted brain image with large cortical infarcts using the whole brain diffeomorphic metric mapping introduced in (16). This framework will incorporate the information of subjects cortical infarcts in the image volume as well as the cortical surface to aid the mapping process. As illustrated in Fig. 4.1, this framework consists of three major processes: 1) whole brain segmentation and the generation of cortical and lateral ventricular surfaces; 2) the extraction of individual anatomical features, including cortical surfaces, gyral and sulcal curves; and 3) individualized large deformation diffeomorphic metric mapping (LDDMM). Fig. 4.2 illustrates the detailed schematic diagram of this individualized whole brain mapping procedure.

4.1 Whole Brain Segmentation and Generation of Cortical and Lateral Ventricular Surfaces

In this stage, the intensity-inhomogeneity corrected T1-weighted MR images of stroke patients (17) were first brought to the Montreal Neurological Institute (MNI) space using the affine transformation with maximizing the cross-correlation of the subjects images with the atlas (18). In MR images, intensity inhomogeneity which are caused by magnetic settings, patients' position, and other factors are not unusual. These steps reduced the effects of intensity-inhomogeneity on input MR images and aligned them to a common space for further downstream processing. After that, FreeSurfer pipeline (19) is applied to reconstruct the inner (white matter) and outer (gray matter) cortical surfaces. The outer surface is constructed by propagating the inner surface to the boundary of gray matter and CSF via a flow with the force based on the image labeling and gradient such that the topologies of the outer and inner surfaces are preserved (19). The inner and outer surfaces are used to represent the geometry of the cortex (see an example in Fig. 4.1B). Notice that the cortical infarcted regions are labeled as CSF in FreeSurfer (red colored mask in Fig. 4.1B).

To overcome the common issue in misalignment of the lateral ventricles due to its extreme enlargement in stroke patients, we also included the lateral ventricle surfaces into our framework (see an example in Fig. 4.1B). We generated the lateral ventricle shapes of each individual subject with properties of smoothness and correct topology by injecting a template shape into them using the LDDMM-image mapping algorithm (20). The lateral ventricle template shape was created from 41 manually labeled lateral ventricles via a large deformation diffeomorphic

template generation algorithm (21). Each lateral ventricle volume was approximated by the transformed template through the LDDMM diffeomorphic map. The mathematical derivation of this template injection procedure and its evaluation on a variety of subcortical structures have been detailed elsewhere (20). This delineation approach had been successfully used to investigate the subcortical shapes in Alzheimer's disease (22), hippocampal shapes in geriatric depression (23), thalamic shape in schizophrenia (24), and the basal ganglia shapes in ADHD (25).

4.2 The Extraction of Individualized Anatomical Features

In this section, we first described the manual extraction of cortical infarct regions from the image as well as the cortical surfaces and then the semi-automated extraction of sulcal/gyral curves from the cortical surfaces. This extraction is done for every stroke patient and its corresponding atlas.

Firstly, a binary mask of the stroke lesion was created manually by depicting the boundaries of the lesion directly into T1 image using FSL View software (26). Based on this mask, we then semi-automatically removed the cortical surfaces using dynamic programming to track the shortest path encompassing the cortical infarcted region within the binary mask (see an example colored in red in Fig. 4.1C) (27). Finally, we then transfer this binary mask to the atlas image using affine transformation in order to mask the corresponding infarcted regions in the atlas space (28).

Next, up to 52 curves (26 curves (i.e. 12 gyri and 14 sulci) for each hemisphere, as shown in Table 4.1 were semi-automatically delineated outside the lesion using dynamic programming (27). These curves are chosen because they are consistently present and easily identifiable on the cortex. The anatomical definitions of these curves are described in Zhong et al., 2010 (10, 29) and online (`http://www.bioeng.nus.edu.sg/cfa/mapping/curveprotocol.html`). Briefly, the initial starting and ending points of each curve are manually defined on the middle surface and the gyral (or sulcal) curve between them is automatically generated using dynamic programming by maximizing (or minimizing) the curvature information along the curve (27). The choice of the curves drawn was limited by the location of the infarct.

4.3 Individualized Large Deformation Diffeomorphic Metric Mapping

In this study, we adopted Large Deformation Diffeomorphic Metric Mapping (LDDMM) algorithm given in (16). We introduced two weight functions to incorporate cortical lesion information in the image volume as well as the cortical surface (as illustrated in Fig. 4.1, lesion mask colored red in both image volume and cortical surface). They helped to exclude the abnormal infarcted brain tissue from the cost function calculation. In addition, we incorporated lateral ventricular surfaces to overcome the common issue in misalignment of the lateral ventricles due to its extreme enlargement in stroke patients.

In the initialization of LDDMM, we identified the momentum values through a

coarse-to-fine multi-manifold LDDMM (MM-LDDMM) cortical surface mappings when the sulcal and gyral curves as well as the middle surface are considered as mapping objects (10, 29), and LDDMM landmark mapping (30). We first smoothed the middle surface in this coarse-to-fine approach. Then, the smooth surface was registered with its sulcal and gyral curves to those of the target using MM-LDDMM described in (10, 29). After that, the paired correspondence points between the target surface and the atlas surface deformed by MM-LDDMM was obtained using the shortest distance criteria, which in turn were being used in the LDDMM-landmark mapping to find the time-dependent momentum that drives the template inner and outer surfaces to those of the target.

After the initialization, LDDMM was performed to seek an optimal diffeomorphic transformation to simultaneously carry these anatomical features from atlas native space to the target brain space. Here, we numerically solved this individualized whole brain mapping problem for target brain with large cortical infarcts with respect to momentum. We first represent the ambient space, $\Omega \subset \mathcal{R}^3$, using a finite number of points, $\Omega \cong \{(x_i^I)_{i=1}^N\} \cup_{i=1}^{n_\gamma} \{(x_j^{\gamma^i})_{j=1}^{N_{\gamma^i}^x}\} \cup_{i=1}^{n_{S_c}} \{(x_j^{S_c{}^i})_{j=1}^{N_{S_c{}^i}^x} \cup_{i=1}^{n_{S_v}} \{(x_j^{S_v{}^i})_{j=1}^{N_{S_v{}^i}^x}\}$ for the atlas coordinates and $\Omega \cong \{(x_i^I)_{i=1}^N\} \cup_{i=1}^{n_\gamma} \{(y_j^{\gamma^i})_{j=1}^{N_{\gamma^i}^y}\} \cup_{i=1}^{n_{S_c}} \{(y_j^{S_c{}^i})_{j=1}^{N_{S_c{}^i}^y} \cup_{i=1}^{n_{S_v}} \{(y_j^{S_v{}^i})_{j=1}^{N_{S_v{}^i}^y}\}$ for the target coordinates. Here, $(x_i^I)_{i=1}^N$ is a regular grid on images $I_{temp}^i(x)$ and $I_{targ}^i(x), i = 1, 2, \cdots, n_I$; $\cup_{i=1}^{n_\gamma}\{(x_j^{\gamma^i})_{j=1}^{N_{\gamma^i}^x}\}$ and $\cup_{i=1}^{n_\gamma}\{(y_j^{\gamma^i})_{j=1}^{N_{\gamma^i}^y}\}$ are the curve sets with respective tangent vectors $w_{x_j}^{\gamma^i}$ of the template and $\tilde{w}_{y_j}^{\gamma^i}$ of the target, where $N_{\gamma^i}^x$ and $N_{\gamma^i}^y$ denote the number of points in the curve γ^i of the template and target respectively. Similarly, $\cup_{i=1}^{n_{s_c}}\{(x_j^{S_c{}^i})_{j=1}^{N_{S_c{}^i}^x}$, $\cup_{i=1}^{n_{s_v}}\{(x_j^{S_v{}^i})_{j=1}^{N_{S_v{}^i}^x}\}$ and $\cup_{i=1}^{n_{s_c}}\{(y_j^{S_c{}^i})_{j=1}^{N_{S_c{}^i}^y}\}$, $\cup_{i=1}^{n_{s_v}}\{(y_j^{S_v{}^i})_{j=1}^{N_{S_v{}^i}^y}\}$ are the cortical surface and lateral ventricular surface sets with respective normal vectors $w_{x_j}^{S^i}$ of the atlas and $\tilde{w}_{y_j}^{S^i}$ of the target, where $N_{S_c{}^i}^x$, $N_{S_v{}^i}^x$ and $N_{S_c{}^i}^y$, $N_{S_v{}^i}^y$ denote the number of

point in the cortical surface ${S_c}^i$ and lateral ventricular surface ${S_v}^i$ of the atlas and target respectively. Lastly, we would like to define currents, $\mu_{\gamma^i_{atlas}}$, $\mu_{S^i_{atlas}}$ and $\mu_{\gamma^i_{targ}}$, $\mu_{S^i_{targ}}$, which are mathematical objects representing curves and surfaces for both atlas and target:

$$\mu_{\gamma^i_{atlas}} = \sum_{j=1}^{N^x_{\gamma^i}} w^{\gamma^i}_{x_j} \otimes \delta_{x_j}$$

$$\mu_{S^i_{atlas}} = \sum_{j=1}^{N^x_{S^i}} w^{S^i}_{x_j} \otimes \delta_{x_j}$$

$$\mu_{\gamma^i_{targ}} = \sum_{j=1}^{N^y_{\gamma^i}} \tilde{w}^{\gamma^i}_{y_j} \otimes \delta_{y_j}$$

$$\mu_{S^i_{targ}} = \sum_{j=1}^{N^y_{S^i}} \tilde{w}^{S^i}_{y_j} \otimes \delta_{y_j}$$

These currents are essentially measure of tangent vectors $w^{\gamma^i}_{x_j}$, $w^{\gamma^i}_{y_j}$ or normal vectors $w^{S^i}_{x_j}$, $w^{S^i}_{y_j}$ evaluated at point x_j/y_j. Putting all these together, the discrete form of energy functional equation can be defined as:

$$
\begin{aligned}
J(\boldsymbol{\alpha_t}) \;=\; & \inf_{\boldsymbol{\alpha(t)}:\dot{\phi}_t = k_V \alpha(t,\phi_t),\phi_0=\mathrm{id}} \int_0^1 \sum_{x_i\in\Omega}\sum_{x_j\in\Omega} \alpha(t,x_i)\cdot k_V(\phi_t(x_i),\phi_t(x_j))\alpha(t,x_j)dt \\
& + \sum_{i=1}^{n_I} \lambda_{I^i} \sum_{j=1}^{N} \left(I^i_{atlas}(\phi_1^{-1}(x_j^I)) - I^i_{targ}(x_j^I)\right)^2 W^i(x_j^I) \\
& + \sum_{i=1}^{n_\gamma} \lambda_{\gamma^i} \left\| \phi_1 \cdot \mu_{\gamma^i_{atlas}} - \mu_{\gamma^i_{targ}} \right\|^2_{k_W^\gamma} \\
& + \sum_{i=1}^{n_{S_c}} \lambda_{{S_c}^i} \sum_{j=1}^{N^x_{S_{c^i}}} \sum_{k=1}^{N^y_{S_{c^i}}} k_w^{S_c}(\hat{x}_j, y_k)[W^{S^i_c}(x_j)\hat{w}^{S^i_c}_{x_j}]\cdot[\tilde{W}^{S^i_c}(y_k)\tilde{w}^{S^i_c}_{y_k}] \\
& + \sum_{i=1}^{n_{S_v}} \lambda_{{S_v}^i} \left\| \phi_1 \cdot \mu_{S^i_{vatlas}} - \mu_{S^i_{vtarg}} \right\|^2_{k_W^{S_v}}, \qquad (4.1)
\end{aligned}
$$

where $\hat{w}^{S^i}_{x_j}$ is the normal vector of transformed surface patch, $\hat{x}_j = \phi_1(x_j), k_W^\gamma, k_W^{S_c}$ and $k_W^{S_v}$ are kernels associated with curves, cortical surfaces and lateral ventricular surfaces respectively, and μ_γ, μ_{S_c} and μ_{S_v} are the currents for curves, cortical surfaces and lateral ventricular surfaces. $W^i(x_j^I)$ is the image weight mask to include only the healthy brain tissue, i.e. inverse of lesion brain mask; $W^{S^i_c}(x_j)$ is the weight mask for the atlas' cortical surface and $\tilde{W}_{S^i_c}(y_k)$ is the weight mask for the subject's cortical surface.

4.4 Quantitative Evaluation of Whole Brain Mapping Accuracy

In order to evaluate the accuracy of our proposed individualized whole brain mapping technique, we have identified several criteria from the literature, which

evaluate properties that are desirable for any such integrative algorithm. In this study, we adopted curve variation to evaluate the alignment of the sulcal and gyral landmarks (30). The surface alignment consistency is used to quantify the alignment in the cortical regions (9). As for the subcortical region, we calculated the Dice overlap ratio of the lateral ventricles and most subcortical structures between the deformed atlas and target. In experiment I, these quantitative measures from the simulated dataset were compared against the quantitative measures from the normal healthy brains, which served as ground truth for us to assess the accuracy of our mapping approach.

4.4.1 Curve Variation

As listed in Table 4.1, a total of 26 curves (12 gyri and 14 sulci per hemisphere) are quantified, subjected to the location and extent of the infarcts. We denoted a specific sulcal/gyral curve of subjects, i and j, in the template coordinates as C^i and C^j. The Hausdorff distance (31) was then computed for these paired curves as

$$d(C^i, C^j) = 0.5\frac{1}{N_1}\sum_{x\in C^i} min_{y\in C^j}|x-y| + 0.5\frac{1}{N_2}\sum_{y\in C^j} min_{x\in C^i}|x-y|$$

where N_1 and N_2 are the number of points on C^i and C^j, respectively. $|x-y|$ denotes the Euclidean distance between points x and y. The first term in the above equation was the average minimum distance of each point in curve C^i to a point in curve C^j, and the second term was the average minimum distance of each point in C^j to a point in C^i.

To evaluate the anatomical variation of a specific sulcal/gyral curve among subjects, which cannot be characterized by the deformation found using the cor-

tical mapping, we further calculated a curve variation error (30) as

$$Var = \frac{1}{2J(J-1)} \sum_{i=1}^{J} \sum_{j=1}^{J} [d(C^i, C^j)]^2$$

where J is the number of subjects in the study. The lower value indicates the better alignment for this curve.

4.4.2 Surface Alignment Consistency

A total of 17 sulcal regions, as listed in Table 4.2, were used in this quantification. Surface alignment consistency (SAC) was initially introduced by (9) for quantifying the anatomical variability of a sulcal region among a group of subjects that can be characterized by the cortical mapping algorithm. Assume J to be the number of subjects involved in the SAC study whose cortical surfaces were transformed to the folded template surface coordinates using the transformation found through one of the cortical mapping algorithms. We considered the sulcal region on the template surface as a reference and denoted its vertex location as x. For every x, we first computed the probability map, $p(x)$, to represent the chance of location x being this sulcal region where $p(x)$ can be approximated as $\frac{i-1}{J-1}$, $i = 1, 2, ..., J$. We then integrated $p(x)$, over the sulcal region and normalized it by this sulcal area of the template surface. In the discrete case where the cortical surface was a triangulated mesh, we can define SAC as

$$SAC = \frac{1}{N} \sum_{i=1}^{J} \frac{i-1}{J-1} n_i$$

where N is the total number of vertices in this sulcal region on the template surface and n_i is the number of of vertices in this sulcal region with probability of $p(x) = \frac{i-1}{J-1}$. SAC is ranged from 0 to 1, i.e. the higher the value, the better the sulcal alignment.

In our study, these 17 sulcal regions (Table 4.2) were manually delineated (see detailed protocol in (10, 29). These sulcal regions were chosen because they are distributed broadly over the cortical surface as illustrated in Fig. 4.3. These sulcal regions were also used for quantifying cortical mapping accuracy in previous studies (9). We computed SAC for each of these seventeen sulcal regions.

4.4.3 Dice Overlap Ratio

To quantify the alignment accuracy of mapping algorithm, we introduce Dice overlap ratio (32). It describes the similarity or overlap between the label of the deformed template D and the one of the target T. We computed the Dice overlap ratio as the intersection of label sets D and T divided by the mean of them:

$$Dice = \frac{D \cap T}{(D+T)/2}$$

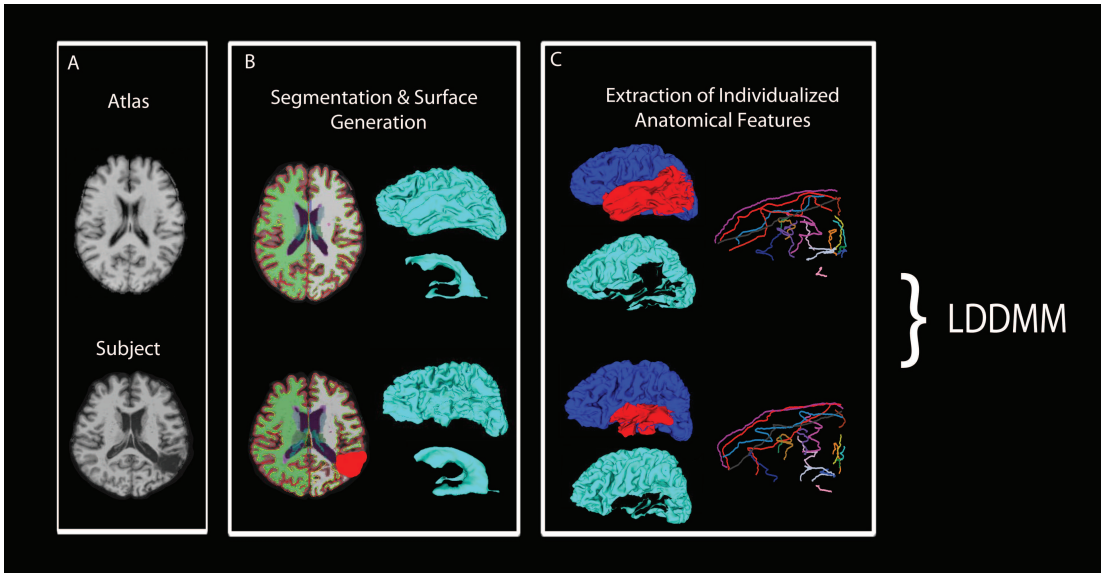

Figure 4.1: Overview of whole individualized diffeomorphic mapping framework. Panel A shows the initial atlas and the subjects brain with large left temporal infarct. Panel B illustrates the preprocessing stages which encompass whole brain segmentation and surfaces generation. Notice the partially missing temporal lobe on the generated cortical surface for the subjects brain. Panel C shows the extraction of individual anatomical features, whereby the curves were selectively delineated around the infarcted region and the portion of cortical infarcted surfaces was removed. These anatomical features were correspondingly extracted for the atlas of each individual stroke patient as well. Lastly, LDDMM was performed to seek an optimal diffeomorphic transformation to simultaneously carry these anatomical features from atlas native space to the subjects brain space.

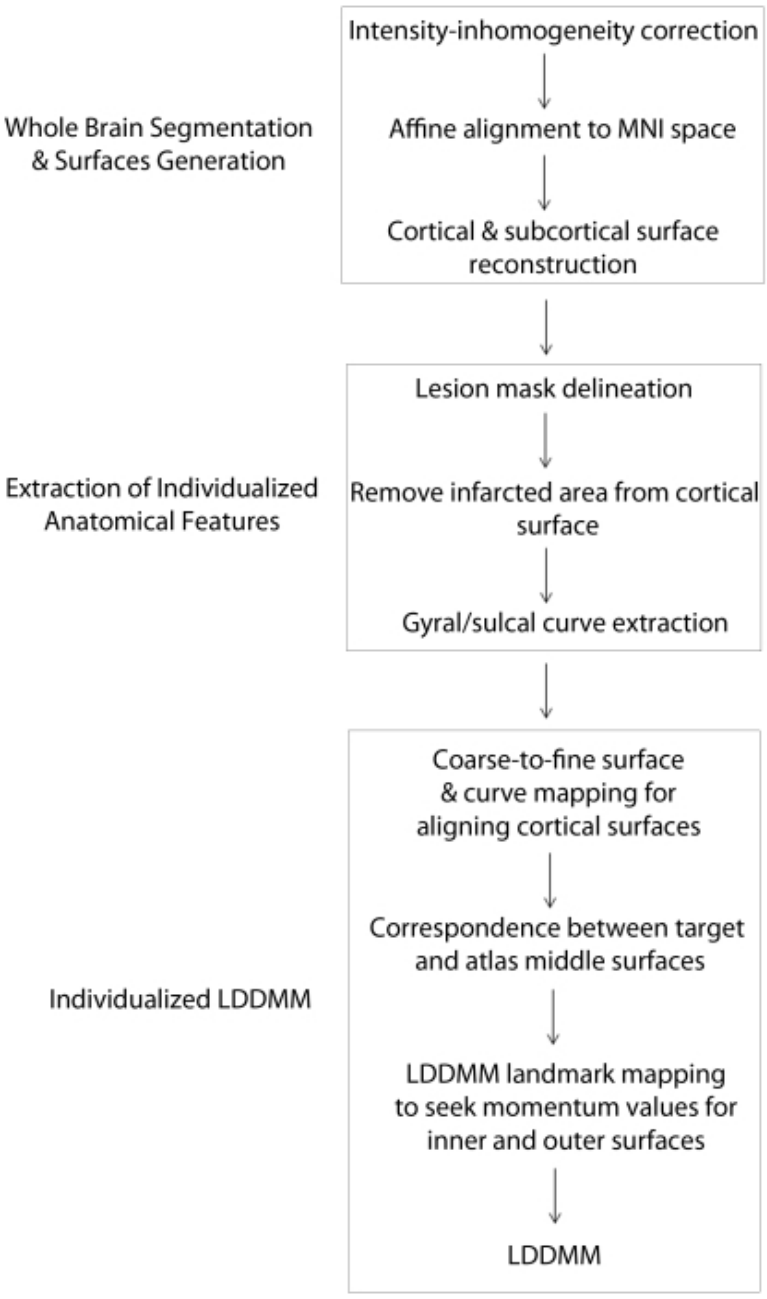

Figure 4.2: Schematic diagram of the individualized whole brain mapping procedure for stroke patients with large cortical infarcts.

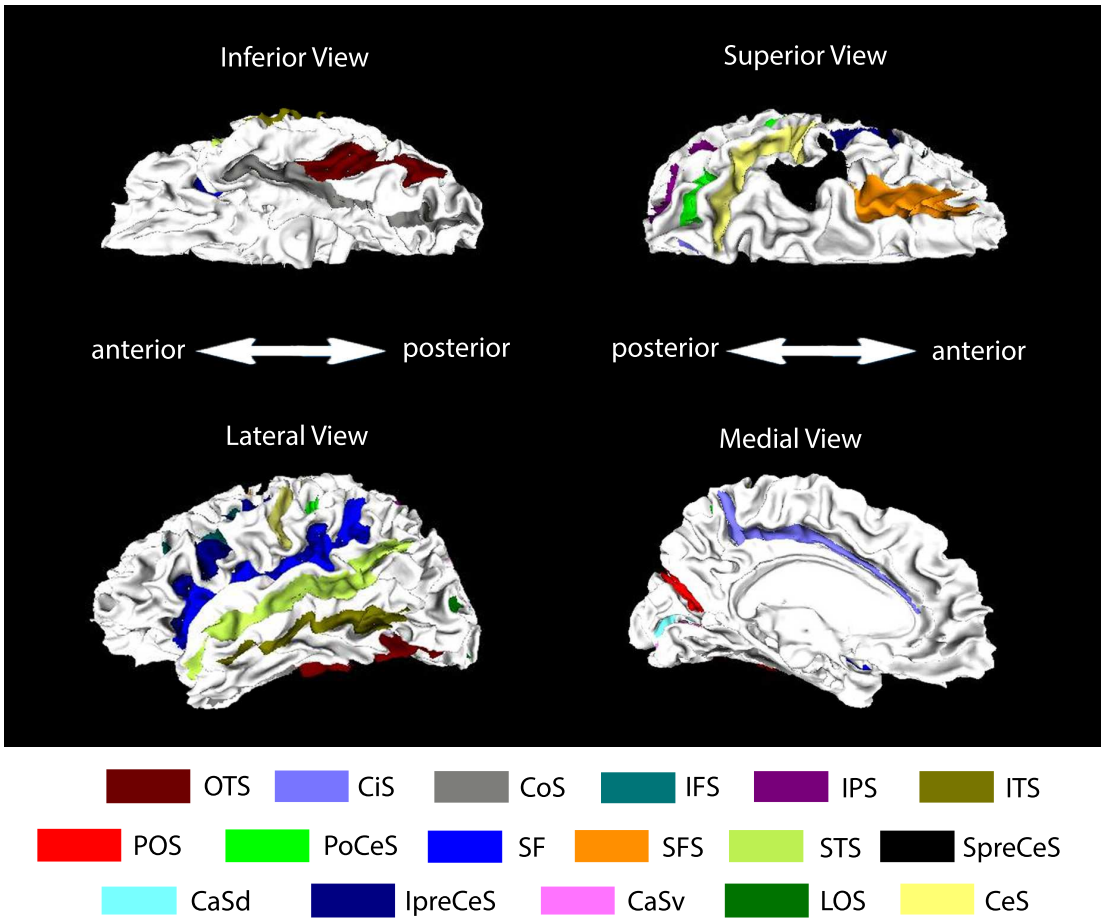

Figure 4.3: Seventeen sulcal regions on superior, inferior, lateral and medial views. Label abbreviations are listed in Table 4.2.

Curves and Abbreviations

Sulcus	Abbreviations	Gyrus	Abbreviations
Superior frontal sulcus	SFS	Precentral gyrus	PreCeG
Inferior frontal sulcus	IFS	Postcentral gyrus	PoCeG
Precentral sulcus	PreCeS	Superior temporal gyrus	STG
Central sulcus	CeS	Middle temporal gyrus	MTG
Postcentral sulcus	PoCeS	Intraparietal gyrus	IPG
Intraparietal sulcus	IPS	Superior frontal gyrus	SFG
Sylvian Fissure	SF	Lateral occipital gyrus	LOG
Anterior segment of the superior temporal sulcus	aSTS	Lingual gyrus	LG
Inferior temporal sulcus	ITS	Cuneus gyrus	CG
Superior callosal sulcus	CC	Anterior border of cuneus gyrus	ACG
Parieto-occipital sulcus	POS	Posterior border of precuneus	PoPreCu
Calcarine sulcus	CaS	Paracentral gyrus	ParaCeG
Olfactory sulcus	OS		
Collateral sulcus	CoS		

Table 4.1: Curves and Abbreviations.

Sulcal surfaces and Abbreviations

Sulcal Regions	Abbreviations
Superior frontal sulcus	SFS
Superior PreCentral Sulcus	SpreCeS
Central Sulcus	CeS
Intraparietal Sulcus	IPS
Occipital Temporal Sulcus	OTS
Superior Temporal Sulcus	STS
Inferior Temporal Sulcus	ITS
Dorsal bank of Calcarine Sulcus	CaSd
Inferior Frontal Sulcus	IFS
Inferior PreCentral Sulcus	IPreCeS
PostCentral Sulcus	PoCeS
Sylvian Fissure	SF
Lateral Occipital Sulcus	LOS
Cingulate sulcus	CiS
Parietal Occipital Sulcus	POS
Collateral Sulcus	CoS
Ventral bank of Calcarine Sulcus	CaSv

Table 4.2: Sulcal Surfaces and Abbreviations.

5

Results

We conducted two experiments using brain images with simulated cortical infarcts and brain images of stroke patients. In the first experiment, we artificially created cortical infarcts in images of healthy brains and then quantified the accuracy of mapping the simulated brain data against that of mapping their corresponding healthy brain data. In the second experiment, we employed our mapping framework to align brains of stroke patients with cortical infarcts and compared the mapping accuracy against that in the first experiment.

5.1 Experiment I: Simulated Lesion

This experiment was designed to assess the quality of our individualized diffeomorphic whole brain mapping approach, in which a cortical infarct is simulated in normal brains. Mapping parameters obtained between the normal and its simulated brains were compared.

10 healthy elderly subjects (mean age: 71.9±6.61; 5 males) from the Open

Access Series of Imaging Studies (OASIS) (33) database were chosen for this experiment, of which, 1 subjects (female, age: 54 years old) was chosen as the atlas for mapping. For OASIS database, MR images collection protocol were reported by Marcus and co-workers in 2007 (33).

5.1.1 Lesion Simulation

Firstly, we identified four stroke patients with unilateral cortical infarction, each at different location across the four main lobes of the brain, i.e. frontal lobe, occipital lobe, temporal lobe and parietal lobe. As illustrated in Fig. 5.1A, the frontal cortical infarct is in the area of left rostral middle frontal cortex and extends to left caudal middle frontal cortex. Fig. 5.1B shows that the occipital cortical infarct is located in the left lingual, cuneus, and lateral-occipital cortices and extends to the left fusiform and parahippocampus. Fig. 5.1C shows that temporal cortical infarct is located in the right superior temporal cortex. Fig. 5.1D illustrates that the parietal cortical infarct is located in the right supramarginal and inferior-parietal cortices.

Then, we created four binary masks in the T1 brain volumes by manually delineating the precise boundaries of each cortical infarctions using FSLView software (26). Next, each of these 4 lesion masks was affine transformed to the 9 healthy elderly brains. It is known that for chronic stroke patients, the infarcted brain tissues would have already been replaced by cerebrospinal fluid (CSF), which is dark in MR T1 modality. Hence, once the lesion masks were affine transformed to the subject space, those voxels which fall into the masks were removed to generate simulated lesioned in those brains, thus yielding 36

artificially simulated stroke brains. Fig. 5.1E-H illustrate examples of the brain images before (top row) and after the simulation (bottom row).

5.1.2 Data Processing

In this experiment, we first employed our mapping approach to align the brain datasets of the nine healthy elderly subjects from the atlas of a healthy elderly subject and considered these mapping as reference for the following comparison. We then applied our mapping approach to align the atlas to the brain datasets of the nine healthy elderly subjects with simulated cortical infarcts. For this, we first delineated anatomical features for each type of cortical infarcts as illustrated in Fig. 5.2. For the cases with simulated frontal cortical infarcts, the infarcted patches of the frontal cortices were first removed from the surfaces, followed by curves delineation. A total of 12 gyri (PreCeG, PoCeG, STG, MTG, IPG, LG, CG, ACG, PoPreCu, SFG, ParaCeG and LOG) and 11 sulci (CeS, PoCS, IPS, SF, aSTS, ITS, CC, POS, CaS, OS, CoS) were intact and hence delineated. For the cases with simulated occipital cortical infarcts, again the infarcted patches of occipital cortices were removed from the surfaces and then 6 gyri (PreCeG, PoCeG, STG, MTG, SFG and ParaCeG) and 9 sulci (SFS, IFS, PreCeS, CeS, PoCeS, SF, aSTS, CC, OS) were delineated as they were on the intact brain tissue. Similarly for the cases with simulated temporal infarcts, surfaces were modified by firstly removed the infarcted temporal cortices, followed by delineating 11 gyri (PreCeG, PoCeG, MTG, IPG, LG, CG, ACG, PoPreCu, SFG, ParaCeG, LOG) and 13 sulci (SFS, IFS, PreCeS, CeS, PoCeS, IPS, SF, ITS, CC, POS, CaS, OS and CoS). Lastly, for the cases with simulated parietal infarcts, the infarcted

parietal cortices were removed from surfaces and 10 gyri (PreCeG, STG, MTG, LG, CG, ACG, PoPreCu, SFG, ParaCeG and LOG) and 10 sulci (SFS, IFS, CeS, aSTS, ITS, CC, POS, CaS, OS and CoS) were delineated.

5.1.3 Quantitative Evaluation

Fig. 5.3 illustrates one example of the mapping results, suggesting that intact brain regions are aligned well while infarcted cortical regions remain unchanged. To quantify the mapping accuracy, we compared the mapping results of the simulated data with those from the original datasets in terms of the goodness of the alignment for gyral/sulcal curves, sulcal regions, and cortical and subcortical regions.

Curve Variation: Fig. 5.4A shows the variation errors of the 23 curves for the simulated frontal infarction cases versus their corresponding healthy brains. Statistically, the mapping of the subjects with the simulated frontal infarcts showed the comparable variation errors for most of the curves ($p>0.05$), except for the sylvian fissure (SF), parietal-occipital sulcus (POS), and lateral occipital gyrus (LOG). Overall, the variation errors averaged across all 23 curves were 7.66 (4.38) for the simulated datas and 7.08 (3.88) for the healthy data.

Fig. 5.4B shows the variation errors of the 15 curves for the simulated occipital infarction cases versus their corresponding healthy brains. Statistically, the mapping of the subjects with the simulated occipital infarcts showed the comparable variation errors for most of the curves ($p>0.05$), except for the superior frontal sulcus (SFS), inferior frontal sulcus (IFS), precentral sulcus (PreCeS), superior temporal sulcus (aSTS), and middle temporal gyrus (MTG). Overall, the

variation errors averaged across all 15 curves were 9.93 (6.40) for the subjects with the simulated data and 8.10 (5.67) for the healthy data.

Fig. 5.4C shows the variation errors of the 24 curves for the simulated temporal infarction cases versus their corresponding healthy brains. Statistically, the mapping of the subjects with the simulated temporal infarcts showed the comparable variation errors for most of the curves ($p>0.05$), except for the middle temporal gyrus (MTG), superior frontal gyrus (SFG), paracentral gyrus (ParaCeG), and lateral occipital gyrus (LOG). Overall, the variation errors averaged across all 24 curves were 8.85 (4.98) for the simulated data and 8.18 (4.76) for the healthy data.

Fig. 5.4D shows the variation errors of the 20 curves for the simulated parietal infarction cases versus their corresponding healthy brains. Statistically, the mapping of the subjects with the simulated parietal infarcts showed the comparable variation errors for most of the curves ($p>0.05$), except for precentral sulcus (CeS), collateral sulcus (CoS), cuneus gyrus (CG), paracentral gyrus (ParaCeG), and lateral occipital gyrus (LOG). Overall, the variation errors averaged across all 20 curves were 9.55 (4.94) for the simulated data and 8.55 (4.81) for the healthy data.

Surface Alignment Consistency(SAC): Fig. 5.5A shows SAC of the 17 sulcal regions for the simulated frontal infarction cases versus their corresponding healthy brains. Statistically, the mapping of the subjects with the simulated frontal infarcts showed the comparable SAC values for most of the sulcal regions ($p>0.05$), except inferior frontal sulcus (IFS), superior frontal sulcus (SFS), and sylvian fissure (SF). Overall, the SAC values averaged across all 17 sulcal regions were 0.30 (0.07) for the subjects with the simulated frontal cortical infarcts and

0.30 (0.07) for the healthy subjects.

Fig. 5.5B shows SAC of the 17 sulcal regions for the simulated occipital infarction versus their corresponding healthy brains. Statistically, the mapping of the subjects with the simulated occipital infarcts showed relatively lower SAC values ($p<0.05$), except collateral sulcus (CoS), inferior temporal sulcus (ITS), occipital temporal sulcus (OTS), and superior preCentral sulcus (SPreCeS). Despite of this tendency, a closer inspection revealed that the magnitude of differences was actually small for these sulcal regions. Overall, the SAC values averaged across all 17 sulcal regions were 0.28 (0.07) for the subjects with simulated occipital cortical infarcts and 0.30 (0.07) for the healthy subjects.

Fig. 5.5C shows SAC of the 17 sulcal regions for the simulated temporal infarction cases versus their corresponding healthy brains. Statistically, the mapping of the subjects with the simulated temporal infarcts showed the comparable SAC values for most of the sulcal regions ($p>0.05$), except inferior frontal sulcus (IFS), superior frontal sulcus (SFS), and sylvian fissure (SF). Overall, the SAC values averaged across all 17 sulcal regions were 0.30 (0.07) for the subjects with the simulated temporal cortical infarcts and 0.30 (0.07) for the healthy subjects.

Fig. 5.5D shows SAC of the 17 sulcal regions for the simulated parietal infarction cases versus their corresponding healthy brains. Statistically, the mapping of the subjects with the simulated parietal infarcts showed the comparable SAC values for most of the sulcal regions ($p>0.05$), except central sulcus (CeS), inferior frontal sulcus (IFS), superior frontal sulcus (SFS), and sylvian fissure (SF). Overall, the SAC values averaged across all 17 sulcal regions were 0.30 (0.07) for the subjects with the simulated parietal cortical infarcts and 0.30 (0.07) for the healthy subjects.

Dice Overlap Ratio: Fig. 5.6 displays the results of Dice overlap ratios for nine brain structures (white matter (CrWM), gray matter (CrCtx), lateral ventricle (LtVent), thalamus (Thal), caudate (Caud), putamen (Put), globus pallidus (Pall), hippocampus (Hipp) and amygdale (Amyg)) for each type of simulated cortical infarct versus their corresponding healthy brains. In all cases, we transferred the manual labels of the atlas along the trajectory of each subject to obtain the automatic labels, and for each subject, we calculated the Dice overlap ratio between the automatic and manual labels.

For the subjects with the simulated frontal cortical infarcts, the Dice overlap ratios are comparable with those of the healthy brains for all 9 structures ($p>0.05$, Fig. 5.6A). The Dice overlap ratios averaged across all 9 structures were 0.83 (0.06) for the subjects with simulated frontal cortical infarcts and 0.83 (0.06) for the healthy subjects.

For the subjects with the simulated occipital cortical infarcts, the Dice overlap ratios are comparable with those of the healthy brains for all 9 structures ($p>0.05$, Fig. 5.6B). The Dice overlap ratios averaged across all 9 structures were 0.81 (0.08) for subjects with the simulated occipital cortical infarcts and 0.83 (0.06) for healthy subjects.

For the subjects with the simulated temporal cortical infarcts, the Dice overlap ratios are comparable with those of the healthy brains for all 9 structures ($p>0.05$, Fig. 5.6C). The Dice overlap ratios averaged across all 9 brain structures were 0.83 (0.06) for subjects with simulated temporal cortical infarcts and 0.83 (0.06) for healthy subjects.

For the subjects with the simulated parietal cortical infarcts, the Dice overlap ratios are comparable with those of the healthy brains for all 9 structures ($p>0.05$,

Fig. 5.6D). The Dice overlap ratios averaged across all 9 brain structures were 0.82 (0.06) for subjects with simulated parietal cortical infarcts and 0.83 (0.06) for healthy subjects.

5.2 Experiment II: Brain Images of Stroke Patients

This second experiment is designed to test the robustness of our mapping approach when dealing with real patients brains with large cortical infarctions. We randomly chose 15 subjects with large cortical infarcts (mean age: 68.67±6.92; 9 males) from the ongoing harmonization cohort recruited by the Memory Aging & Cognition Center (MACC) at the National University of Singapore. These MR images were collected on a 3T Siemens Magnetom Trio Tim Scanner using a 32-channel head-coil at the Clinical Imaging Research Center of the National University of Singapore. High resolution T1-weighted Magnetization Prepared Rapid Gradient Recalled Echo (MPRAGE) images were acquired with 192 slices, 1mm thickness, in-plane resolution 1 mm, no inter-slice gap, sagittal acquisition, field of view = 256 x 256 mm, matrix = 256 x 256, repetition time = 2300ms, echo time = 1.9 ms, inversion time = 900 ms, flip angle = 9°.

5.2.1 Lesion Location

Fig. 5.7 shows the brains of stroke patients in Experiment II. Starting from top left and going clockwise the location of cortical infarcts are: 1) right temporal-parietal infarct, 2) left temporal-parietal-occipital infarct, 3) right frontal infarct,

4) right temporal-parietal infarct, 5) left temporal-parietal-occipital infarct, 6) right frontal-temporal-parietal infarct, 7) right frontal infarct, 8) left temporal infarct, 9) right temporal-parietal infarct, 10) left temporal parietal infarct, 11) right parietal-temporal-occipital infarct, 12) right temporal infarct, 13) left frontal infarct, 14) right frontal infarct, 15) right frontal infarct. These cortical infarctions varied with location and extent of the lesion. Some with infarcts constrained within a single lobe, while others large infarcts spread across different lobes of the brain.

5.2.2 Data Processing

Similar to experiment 1, we aligned the atlas (Fig. 5.8A) to the brain of the 15 stroke subjects using our mapping approach. For this, we customized the anatomical features used in our individualized mapping approach for each subject since cortical infarcts are at different anatomical locations. Taking brain 4 in Fig. 5.7 as an example, we described our data processing in details. First, a binary mask of the infarcted region was created manually at the location of the temporal and parietal lobes in the subject space (Fig. 5.8B and C). We then aligned the atlas image to the subjects image based on affine transformation and transferred the subjects binary mask to the atlas in order to mask the corresponding anatomical infarct region in the atlas space. Third, we automatically removed the cortical surface in the binary mask in both the atlas and the subject spaces. Subsequently, a total of 10 gyri (PreCeG, PoCeG, MTG, LG, CG, ACG, PoPreCu, ParaCeG, SFG and LOG) and 12 sulci (IFS, PreCeS, CeS, IPS, aSTS, ITS, CC, OS, SFS, POS, CaS, and CoS) were delineated in the cortical surfaces of the atlas and the

subject as these curves were in the intact cortical region (Fig. 5.8 10 D and E). Finally, these anatomical features, including the image volume, cortical surface, and gyral/sulcal curves were used in our individualized diffeomorphic mapping framework. Fig. 5.9 illustrates the example of the mapping.

5.2.3 Quantitative Evaluation

We used the same quantitative measures as in experiment 1 (i.e. curve variation error, surface alignment consistency and Dice overlap ratio) to evaluate the mapping results of the 15 stroke subjects in Experiment 2. For this, we compared these three measures in Experiment 2 with those from the simulated data in Experiment 1.

Curve Variation: Fig. 5.10A illustrates the variation errors of the 26 curves for the stroke subjects. Due to distinct infarct locations, not all 26 curves could be indentified in the stroke brains and they were considered as missing data. The superior callosal sulcus (CC) and olfactory sulcus (OS) were observed in all 15 subjects. Two-sample t-tests revealed that the variation errors of the 26 curves of the stroke subjects were comparable with the results of the simulated stroke cases in experiment 1 (stroke versus simulated frontal, p=0.606; stroke versus simulated occipital, p=0.585; stroke versus simulated temporal, p=0.823; stroke versus simulated parietal, p=0.738).

Surface Alignment Consistency(SAC): Similarly, the SAC values of the same 17 sulcal regions (Table 4.2) were illustrated in Fig. 5.10B. Due to distinct infarct locations, not all 17 sulcal regions could be indentified in the stroke brains and they were considered as missing data. Only 5 sulcal regions (supe-

rior frontal sulcus, superior pre-central sulcus, central sulcus, inferior pre-central sulcus and cingulated sulcus) were intact throughout all 15 stroke subjects. Compared to the simulated infarct cases in experiment 1, two-sample t-test conducted failed to show statistically different ($p>0.05$) in the results from both experiments (stroke versus simulated frontal, $p=0.160$; stroke versus simulated occipital, $p=0.266$; stroke versus simulated temporal, $p=0.230$; stroke versus simulated parietal, $p=0.212$).

Dice Overlap Ratio: Fig. 5.10C shows the Dice overlap ratios for the 9 brain structures. Two-sample t-tests failed to show statistically different ($p>0.05$) in the results from both experiments (stroke versus simulated frontal cortical infarcts, $p=0.075$; stroke versus simulated occipital cortical infarcts, $p=0.277$; stroke versus simulated temporal cortical infarcts, $p=0.069$; stroke versus simulated parietal cortical infarcts, $p=0.103$).

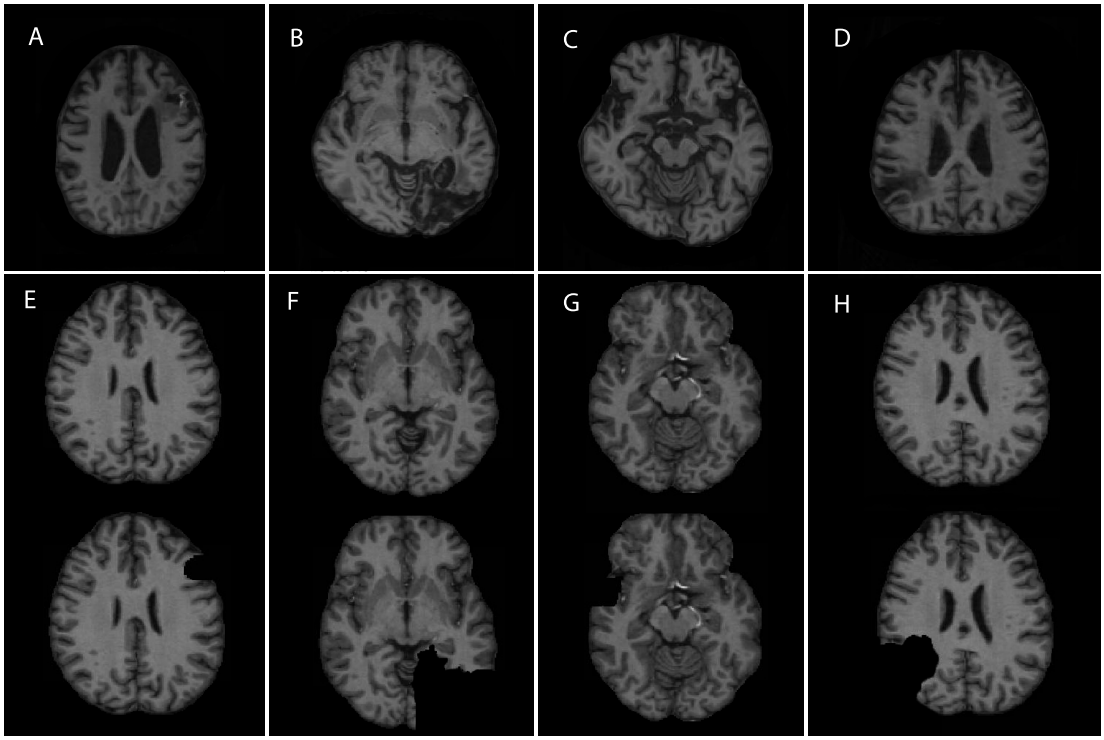

Figure 5.1: Four stroke patients brains with unilateral cortical infarcts used in experiment 1 (A)-(D). Example of 4 simulated cortical infarctions in a normal brain (E)-(H). Panel (E) shows a slice from axial view of normal brain, and the same slice with simulated left frontal cortical infarction inserted. Similarly, panel (F)-(H) illustrate a different slice view of the same normal brain, with cortical infarctions in 3 other lobes inserted, i.e. left occipital, right temporal and right parietal lobes.

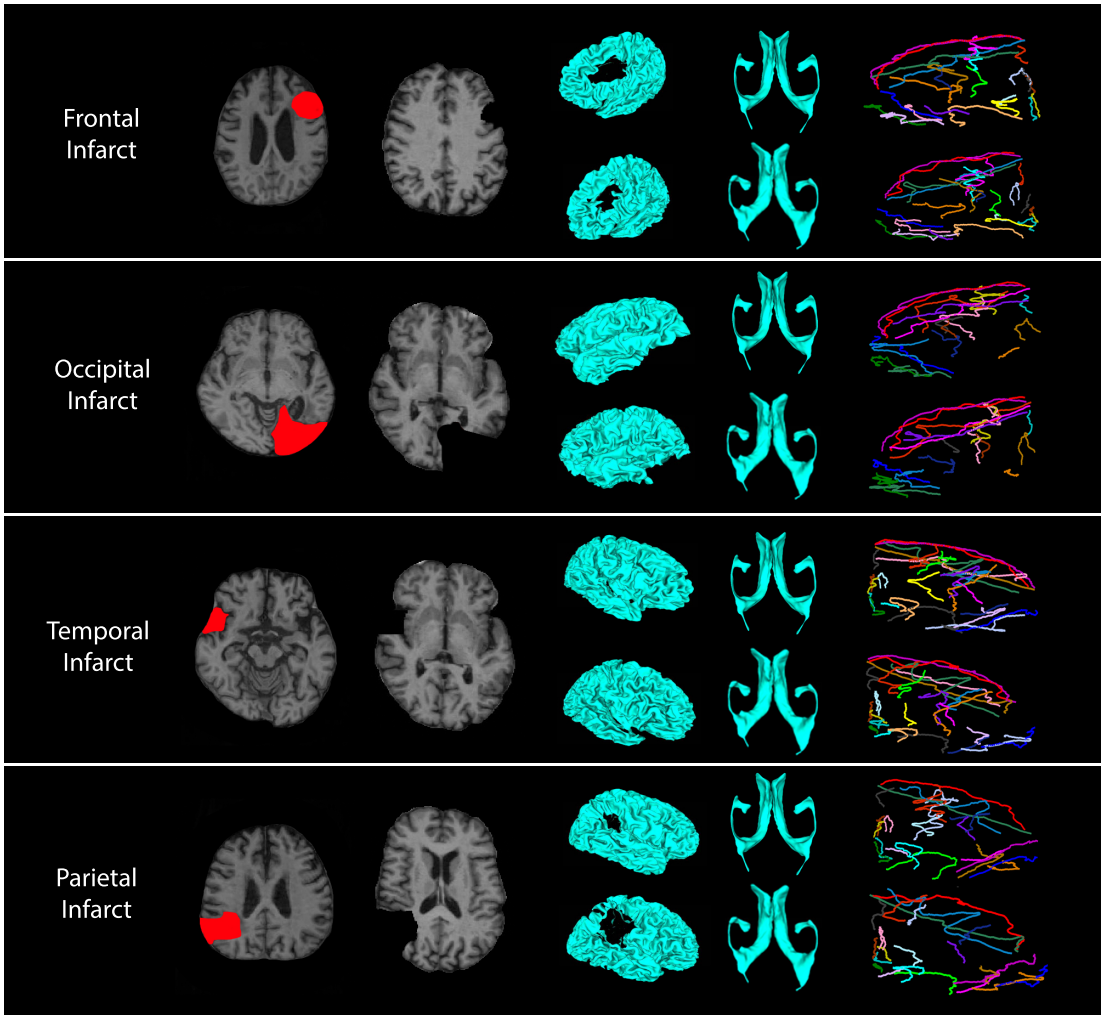

Figure 5.2: Brains with simulated cortical infarcts and their anatomical features extracted for mapping. Each row shows one type of simulated cortical infarct cases. In each row, the lesion mask was colored in red in the original stroke patients brains, and the anatomical features extracted from atlas were displayed at the top of each row while the anatomical features extracted from subject were displayed at the bottom of each row.

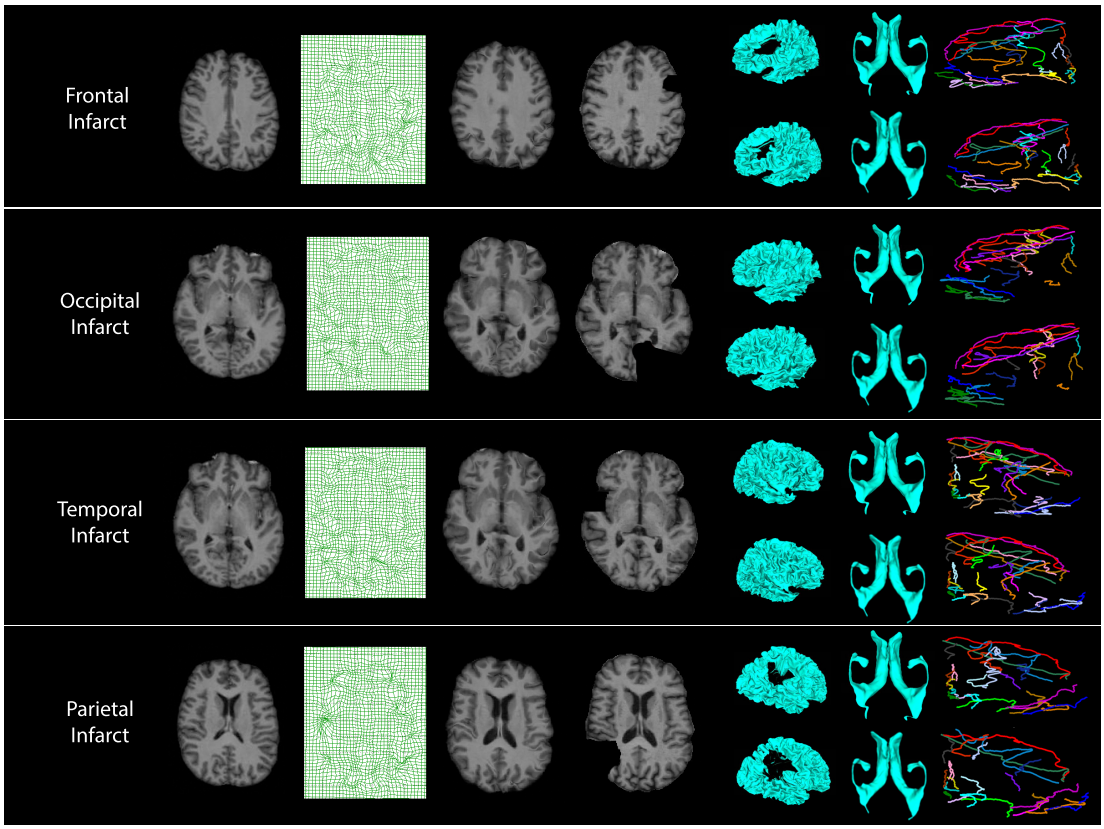

Figure 5.3: Mapping results of experiment 1. Each row depicts the mapping results for one type of simulated cortical infarcts. In each row: atlas, displacement field, deformed atlas and subjects image with simulated infarct were shown from left to right. The anatomical features of deformed atlas were displayed at the top of each row and the anatomical features of subject were shown at the bottom of each row.

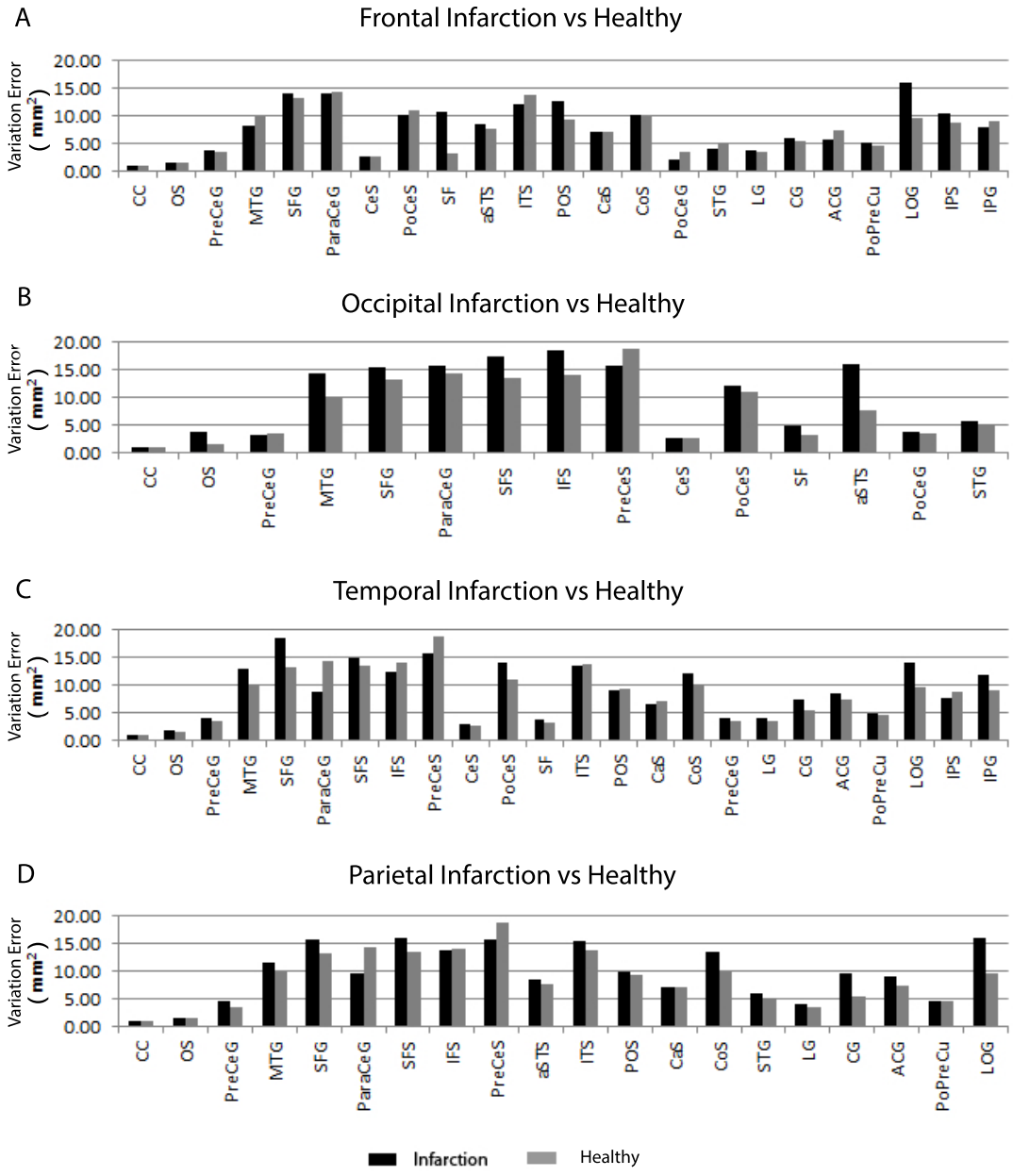

Figure 5.4: The variation errors of the curves for all four cases of simulated cortical infarcts in experiment 1. Due to distinct infarct locations, the number of curves involved in each case varies: 23 curves for subjects with simulated frontal infarct, 15 curves for subjects with simulated occipital infarct, 24 curves for subjects with simulated temporal infarct and 20 curves for subjects with simulated parietal infarct. Label abbreviations are listed in Table 4.1.

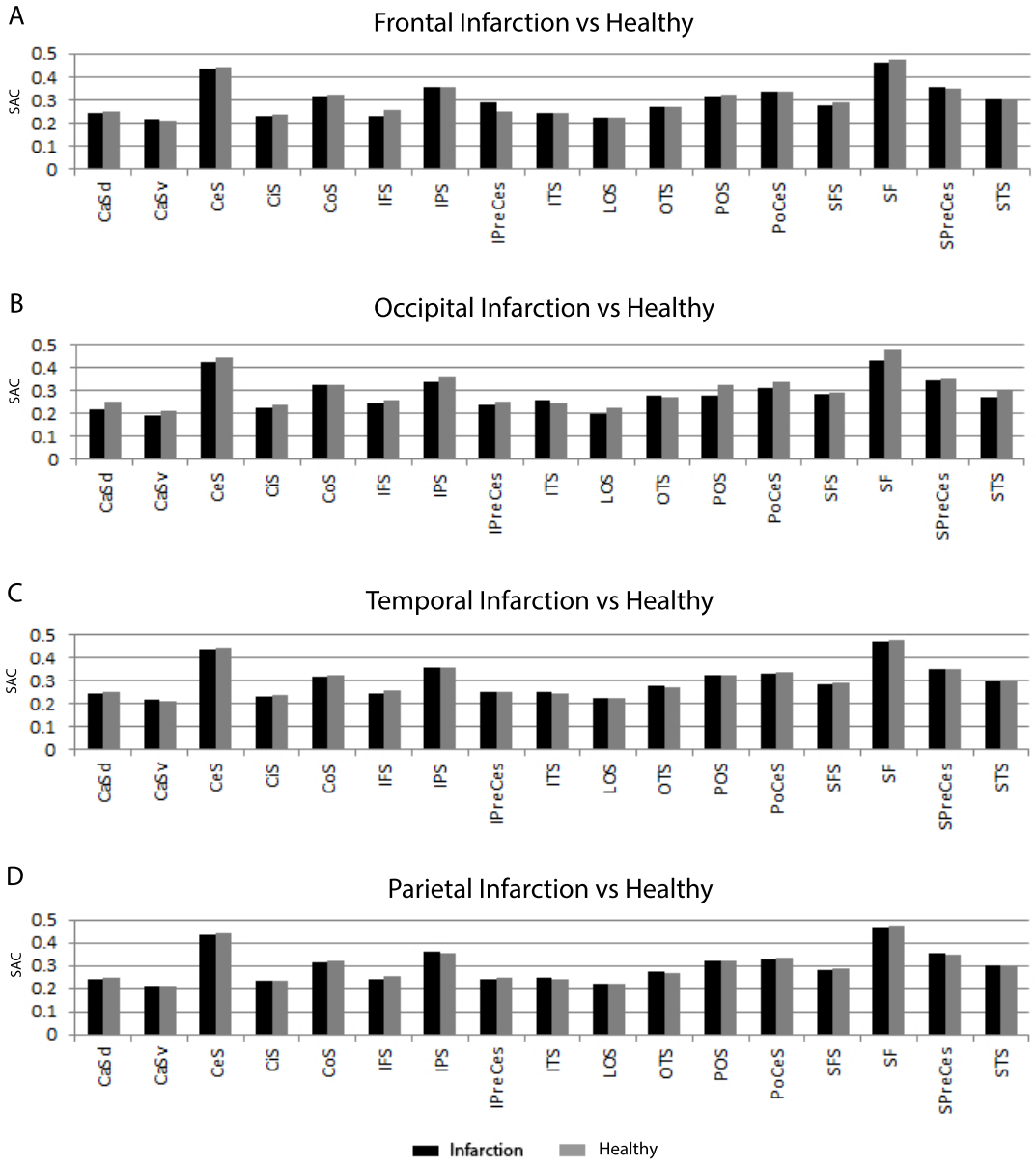

Figure 5.5: The surface alignment consistencies for 17 sulcal regions in experiment 1. Label abbreviations are listed in Table 4.2.

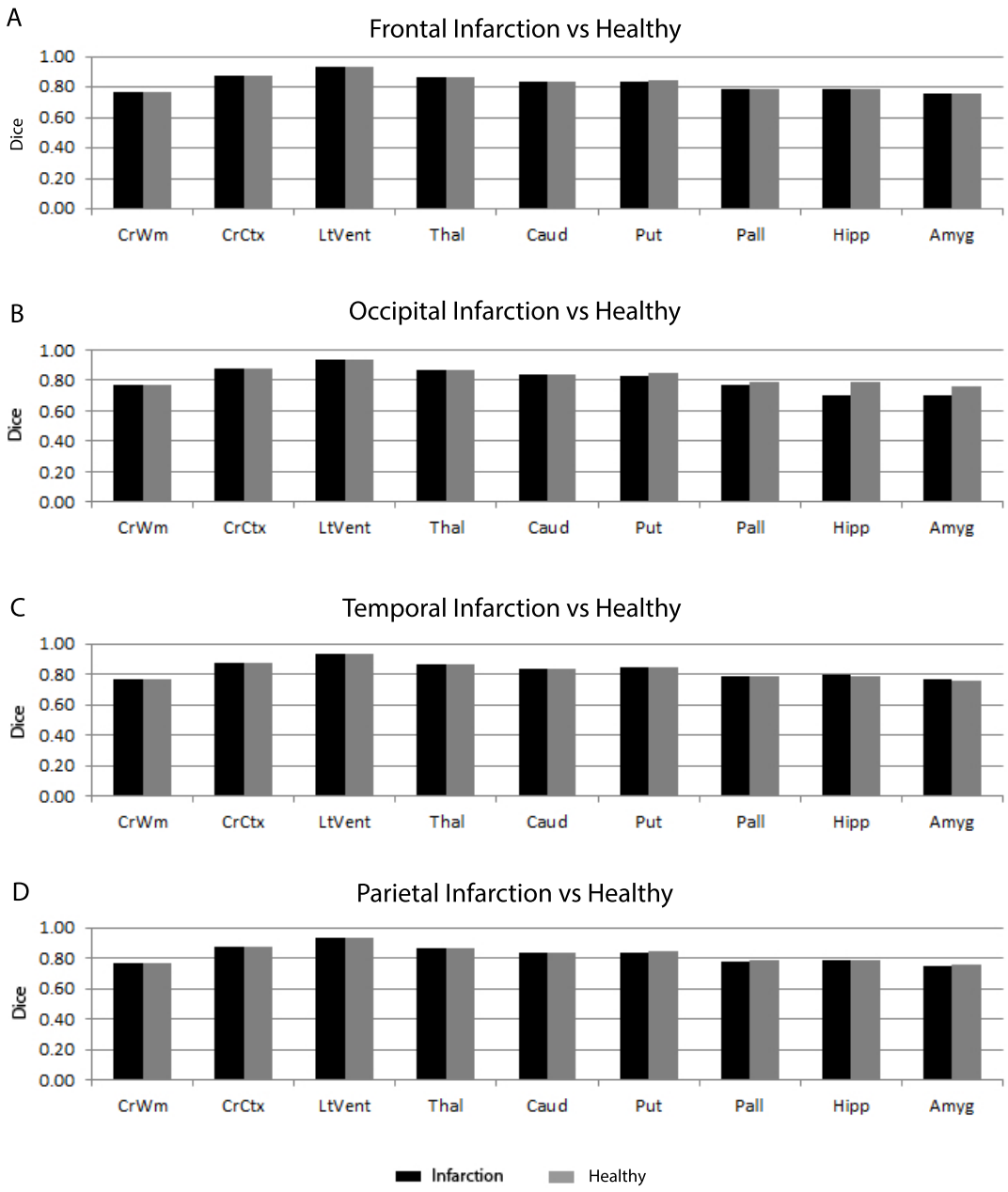

Figure 5.6: The Dice overlap ratio in experiment 1. The segmentation labels are: cerebral white matter (CrWm), cerebral cortex (CrCtx), lateral ventricle (LtVent), thalamus proper (Thal), caudate (Caud), putamen (Put), pallidum (Pall), hippocampus (Hipp), amygdala (Amyg).

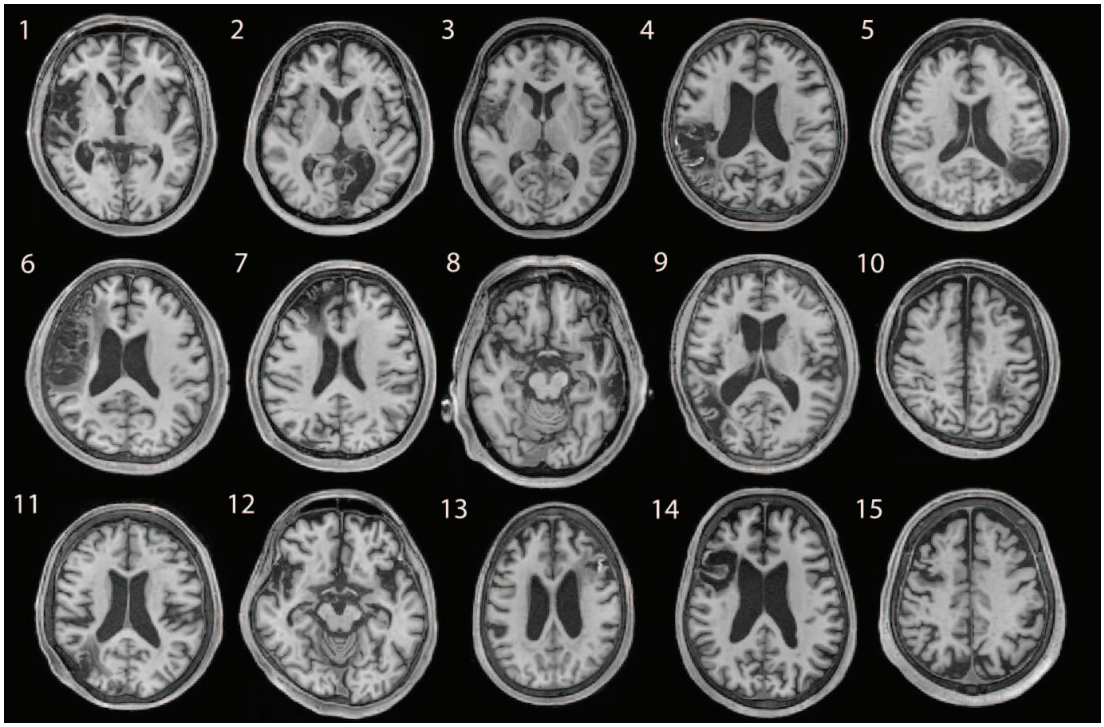

Figure 5.7: Brains of stroke patients in Experiment 2. Starting from top left and going clockwise the location of cortical infarcts are: 1) right temporal-parietal infarct, 2) left temporal-parietal-occipital infarct, 3) right frontal infarct, 4) right temporal-parietal infarct, 5) left temporal-parietal-occipital infarct, 6) right frontal-temporal-parietal infarct, 7) right frontal infarct, 8) left temporal infarct, 9) right temporal-parietal infarct, 10) left temporal parietal infarct, 11) right parietal-temporal-occipital infarct, 12) right temporal infarct, 13) left frontal infarct, 14) right frontal infarct, 15) right frontal infarct.

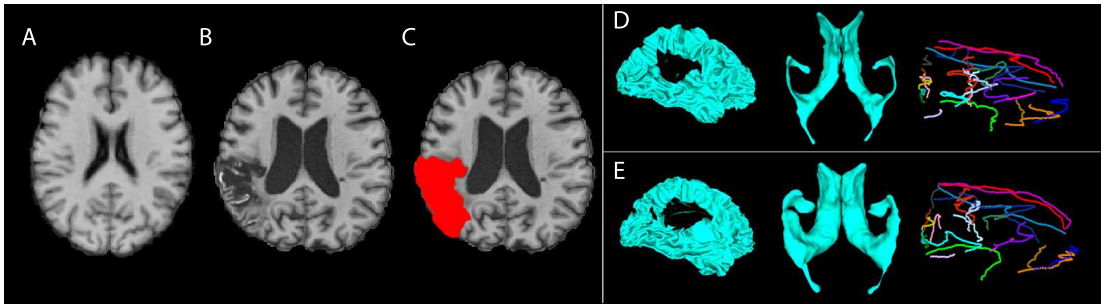

Figure 5.8: Example of image volume and anatomical features extracted for mapping in experiment 2. (A) Atlas image volume. (B) Stroke patients brain (brain 4 in Figure 5.7). (C) Stroke brain with red colored lesion mask. (D) Anatomical features extracted from atlas for mapping. (E) Anatomical features extracted from subject for mapping.

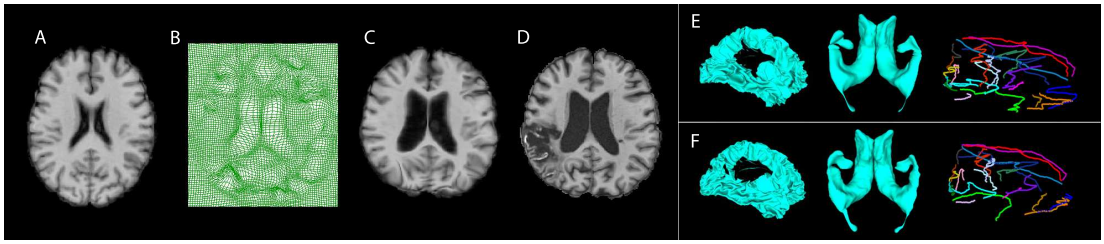

Figure 5.9: Example of mapping results in experiment 2. (A) Atlas image volume. (B) Displacement field of deformed atlas. (C) Deformed atlas image volume. (D) Stroke patients brain (brain 4 in Figure 9). (E) Anatomical features of deformed atlas. (F) Anatomical features of subject.

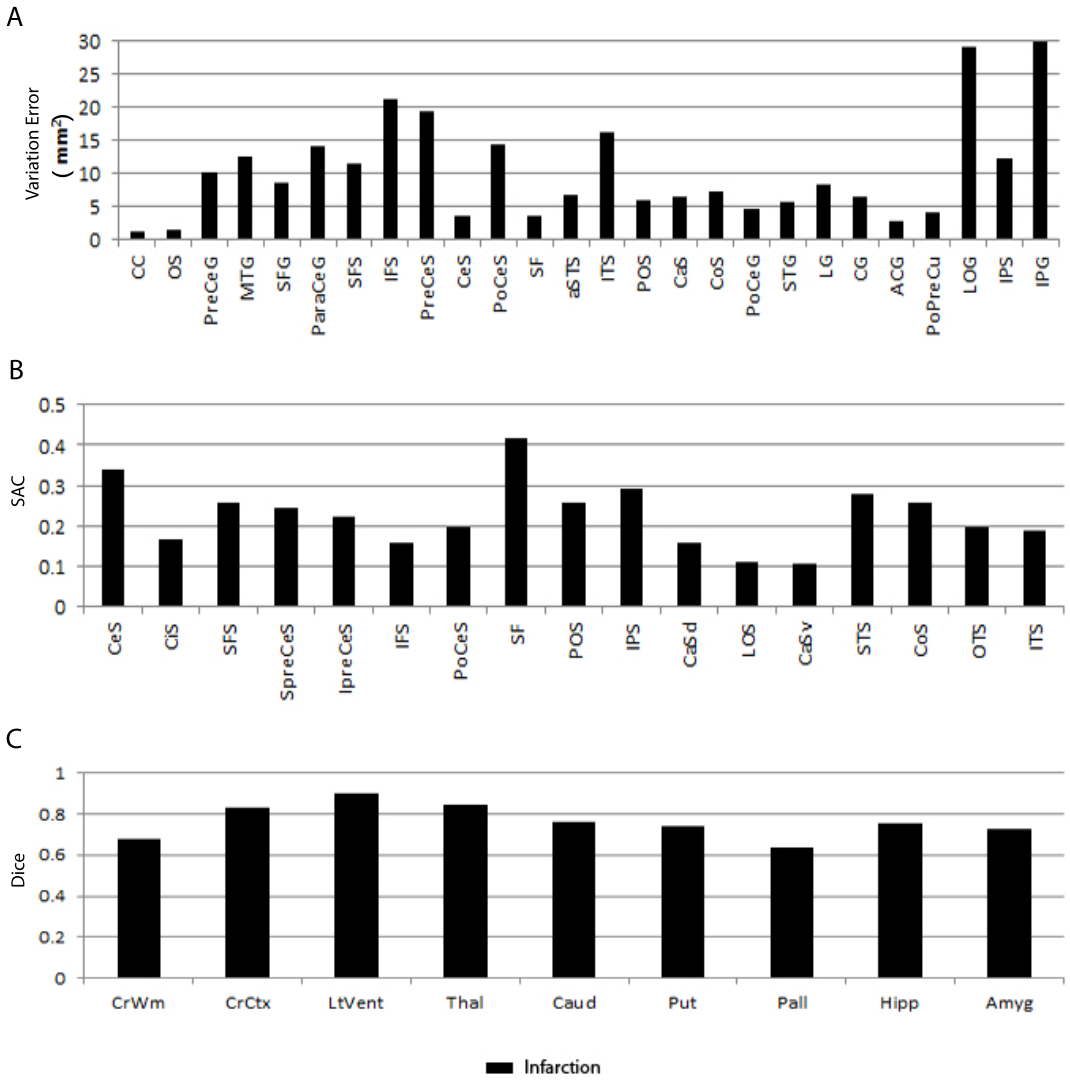

Figure 5.10: Quantitative measures used for validation in experiment 2. Due to different infarct locations, those subjects with missing curves and sulcal regions were considered as missing data. Only 2 curves (CC and OS) and 5 sulcal regions (SFS, SPreCes, CeS, IPreCeS and CiS) prevailed in all 15 stroked brains. Label abbreviations are listed in Table 4.1 (curves) and Table 4.2 (sulcal regions).

6

Discussion

This study revisited whole brain mapping for stroke patients with large cortical infarcts using the previously established LDDMM whole brain mapping (16) in an individualized setting with cost function masking (1). Our results revealed that this proposed individualized whole brain mapping for patients with large cortical infarcts produced comparable accuracy with LDDMM for healthy brains (16).

Cost function masking is still necessary when dealing with brains with large cortical infarcts for whole brain mapping (5). In our individualized setting, there are three manual interventions in the step of extraction of individualized anatomical features: (1) mask delineation for cortical infarcted tissue; (2) removal of the infarcted patch from cortical surfaces for both atlas and target; (3) curves delineation for those intact portions of the brain for both atlas and target. These manual interventions were needed because the lesion mask helped to exclude the cortical infarcted tissue from the cost function calculation. Then, removal of the infarcted surface area ensured that only the intact surface area was used for

finding the correspondence points between the atlas and target. Curves were delineated on an individualized basis to help in whole brain mapping as well.

To test the robustness of our proposed method, the simulated dataset generated should be as generalized as possible to cover all forms of cortical infarction. With this aim in mind, we chose 9 healthy elderly subjects from the OASIS database, and artificially inserted each of them with cortical infarctions across 4 main lobes of the brain. The advantage of using this database is that it contains the manual segmentation labels for both cortical and subcortical regions for evaluation. In order to verify our method was indeed location invariant and accurate for both cortical and subcortical structures, 3 quantitative measures were selected (i.e. curve variation error, surface alignment consistency, and Dice overlap ratio) for verification. Results showed that for curve variation error, the measures obtained between individualized LDDMM on simulated dataset and LDDMM on original healthy brains were in general close to each other. Statistics conducted failed to show significant difference between the means of curve variation error for both approaches, except for the case of simulated occipital infarction dataset ($p<0.05$). This is because the simulated occipital infarct has an extremely large area of infarction, causing the mapping error to increase steeply due to significant decrease in volume of the brain from which the mapping parameters are derived. Besides, we also realized that in this particular case, the two cortical curves (i.e. middle temporal gyrus and superior temporal sulcus) which were just next to the lesion could potentially be affected since their curve variation errors were much higher as compared to the rest of the curves. Recalculate the statistics with these two curves removed failed to show statistically different in means of both individualized LDDMM and normal LDDMM. As for surface alignment

consistency, we can see that both approaches produced similar accuracies for all 17 sulcal regions, suggesting overall good alignment of cortical surfaces. Statistics conducted again failed to show significant difference between the means of SAC values for both individualized LDDMM and normal LDDMM ($p>0.05$), except for the cases of simulated occipital and temporal cortical infarction ($p<0.05$). To explain such findings, we examined the data in both cases and discovered that though the absolute differences in SAC values were small between the healthy and simulated brains, but most of the normal brains surfaces have slightly higher SAC values, hence deviated the means of both groups and yielded such results. The results for Dice overlap ratio showed that all 9 brain structures are consistent for both approaches as well, implying good mapping for both cortical (i.e. gray and white matter) and subcortical (lateral ventricle, thalamus, caudate, putamen, globus pallidus, hippocampus and amygdale) structures. Although the statistics conducted showed significant difference ($p<0.05$) in the means between the simulated parietal infarcted brains and normal brains, we believed that this is again due to the trend in which dice indices of the healthy brains were mostly slightly higher than the dice indices of the simulated parietal infarcted brains. The absolute difference both groups Dice indices were small. Hence, based on the results of these quantitative measures we concluded that our proposed individualized diffeomorphic whole brain mapping is as accurate as the LDDMM whole brain mapping for healthy brains and it is location invariant.

In the second experiment, we dealt with real patients brains with large cortical infarcts chosen from the MACC database. These stroke patients come with a variety of cortical infarction pathology showing the heterogeneous nature of these infarctions. We built our probabilistic atlas from a pool of carefully chosen sub-

jects from MACC database. The probabilistic atlas further improves the mapping accuracy by constructing a brain atlas similar to those of the subjects involved in the study, such that it eliminates unnecessary deformation due to group differences, and is thus capable of capturing the anatomical variations of the MACC population. Two selection criteria were used when selecting subjects for atlas generation: (1) WMH; (2) No cortical infarction. WMH measure was employed because it is thought to reflect small vessel cerebrovascular disease (34, 35), and may contribute to age-associated cognitive decline (36, 37), and increased risk of dementia (38). Besides, the probabilistic atlas should be generalized to cater for all kinds of target brains with different cortical infarcts. Hence, all subjects chosen would have to be free from cortical infarction. Next, the effect of lesion mask was made clear in Fig. 5.9, in which the deformation field for the infarcted area was preserved; only those intact brain areas outside the lesion mask were subjected to deformation. When using the same three quantitative measures to assess the quality of our individualized whole brain mapping, we noticed that they produced similar results to that of the healthy brains in experiment I. Statistics conducted failed to show any statistically different in means of these measures for both groups. Hence, these findings suggested that our individualized diffeomorphic whole brain mapping approach is able to register well the intact portion of the brains despite the existence of large cortical infarcts.

7

Conclusion

In conclusion, we have established a brain mapping framework that incorporates the whole brain LDDMM algorithm with individualized anatomical features, such as cortical surfaces, sulcal/gyral curves, surfaces of the lateral ventricles, and image volume intensity. Based on the experiments conducted, it has been showed that the proposed framework is able to 1) mask out cortical infarct regions; 2) well constrain the boundary of cortical infarcts; 3) well align anatomical features in the intact brain regions. Results from quantitative validation showed that our proposed whole brain mapping framework for stroke patients produces comparable results to the previously established LDDMM whole brain mapping for normal brains.

8

Future Work

There is still quite a bit of potential development for this work. Since manual interventions such as lesion mask and anatomical landmark delineation are inevitable in the current approach, future development to make this framework fully automatic would be ideal. By making this framework automatic will increase the efficiency by shortening the processing time, rid operators from frustrations of manual labour, and decrease inter-operator variability.

Instead of restricting to cortical infarcts, another potential future development will be to extend this approach for infarcts at other locations of the brain such as subcortical region and cerebellum.

References

[1] Matthew Brett, Alexander P. Leff, Chris Rorden, and John Ashburner. Spatial normalization of brain images with focal lesions using cost function masking. *NeuroImage*, 14(2):486 – 500, 2001. 1, 4, 44

[2] Parashkev Nachev, Elizabeth Coulthard, H. Rolf Jger, Christopher Kennard, and Masud Husain. Enantiomorphic normalization of focally lesioned brains. *NeuroImage*, 39(3):1215 – 1226, 2008. 3

[3] D. Kimura. The asymmetry of the human brain. *Sci Am*, 228:70–8, 1973. 4

[4] John Ashburner and Karl J. Friston. Unified segmentation. *NeuroImage*, 26(3):839 – 851, 2005. 4

[5] Sarah M. Andersen, Steven Z. Rapcsak, and Plagie M. Beeson. Cost function masking during normalization of brains with focal lesions: Still a necessity? *NeuroImage*, 53(1):78 – 84, 2010. 4, 44

[6] Bruce Fischl, Martin I. Sereno, and Anders M. Dale. Cortical surface-based analysis: Ii: Inflation, flattening, and a surface-based coordinate system. *NeuroImage*, 9 (2):195 – 207, 1999. 5

[7] David C. Van Essen, Heather A. Drury, Sarang Joshi, and Michael I. Miller. Functional and structural mapping of human cerebral cortex: Solutions are in thesurfaces. *Proceedings of the National Academy of Sciences*, 95(3):788–795, 1998. 5

[8] Marc Vaillant, Anqi Qiu, Joan Glauns, and Michael I. Miller. Diffeomorphic metric surface mapping in subregion of the superior temporal gyrus. *NeuroImage*, 34(3): 1149 – 1159, 2007. 5

[9] David C. Van Essen. A population-average, landmark- and surface-based (pals) atlas of human cerebral cortex. *NeuroImage*, 28:635–662, 2005. 5, 15, 16, 17

[10] Jidan Zhong and Anqi Qiu. Multi-manifold diffeomorphic metric mapping for aligning cortical hemispheric surfaces. *NeuroImage*, 49:355–365, 2010. 5, 11, 12, 17

[11] Alan Anticevic, Donna L. Dierker, Sarah K. Gillespie, Grega Repovs, John G. Csernansky, David C. Van Essen, and Deanna M. Barch. Comparing surface-based and volume-based analyses of functional neuroimaging data in patients with schizophrenia. *NeuroImage*, 41(3): 835 – 848, 2008. 5

[12] G. Postelnicu, L. Zollei, and B. Fischl. Combined volumetric and surface registration. *Medical Imaging, IEEE Transactions on*, 28(4):508 –522, april 2009. 5

[13] Anand Joshi, David Shattuck, Paul Thompson, and Richard Leahy. Brain image registration using cortically constrained harmonic mappings. 4584:359–371, 2007. 5

[14] Shattuck D.W. Thompson P.M. Leahy R.M. Joshi, A.A. Surface-constrained volumetric brain registration using harmonic mappings. *Medical Imaging, IEEE Transactions on*, 26:1657–1669, 2007. 5

[15] Dinggang Shen and C. Davatzikos. Hammer: hierarchical attribute matching mechanism for elastic registration. *Medical Imaging, IEEE Transactions on*, 21(11): 1421 –1439, nov. 2002. 5, 6

[16] Jia Du, Laurent Younes, and Anqi Qiu. Whole brain diffeomorphic metric mapping via integration of sulcal and gyral curves, cortical surfaces, and images. *NeuroImage*, 56(1):162 – 173, 2011. 5, 7, 8, 11, 44

[17] J.G. Sled, A.P. Zijdenbos, and A.C. Evans. A nonparametric method for automatic correction of intensity nonuniformity in mri data. *Medical Imaging, IEEE Transactions on*, 17(1):87 –97, feb. 1998. 9

[18] M. Jenkinson and S. Smith. A global optimisation method for robust affine registration of brain images. *Med Image Anal*, 5:143–156, 2001. 9

[19] Anders M. Dale, Bruce Fischl, and Martin I. Sereno. Cortical surface-based analysis: I. segmentation and surface reconstruction. *NeuroImage*, 9(2):179 – 194, 1999. 9

[20] A. Qiu and M. I. Miller. Multi-structure network shape analysis via normal surface momentum maps. *NeuroImage*, 42:1430 – 1438, 2008. 9, 10

[21] Anqi Qiu, T. Brown, B. Fischl, Jun Ma, and M.I. Miller. Atlas generation for subcortical and ventricular structures with its applications in shape analysis. *Image Processing, IEEE Transactions on*, 19(6):1539–1547, 2010. 10

[22] Anqi Qiu, Christine Fennema-Notestine, Anders M. Dale, and Michael I. Miller. Regional shape abnormalities in mild cognitive impairment and alzheimer's disease. *NeuroImage*, 45(3):656 – 661, 2009. 10

[23] Anqi Qiu, Warren D. Taylor, Zheen Zhao, James R. MacFall, Michael I. Miller, Cynthia R. Key, Martha E. Payne, David C. Steffens, and K. Ranga R. Krishnan. {APOE} related hippocampal shape alteration in geriatric depression. *NeuroImage*, 44(3):620 – 626, 2009. 10

[24] Anqi Qiu, Jidan Zhong, Steven Graham, Ming Ying Chia, and Kang Sim. Combined analyses of thalamic volume, shape and white matter integrity in first-episode schizophrenia. *NeuroImage*, 47(4):1163 – 1171, 2009. 10

[25] M. Adler E. M. Mahone M. B. Denckla M. I. Miller A. Qiu, D. Crocetti and S. H. Mostofsky. Basal ganglia volume and shape in children with attention deficit hyperactivity disorder. *Am J Psychiatry*, 166:74 – 82, Jan 2009. 10

[26] Mark Jenkinson, Christian F. Beckmann, Timothy E.J. Behrens, Mark W. Woolrich, and Stephen M. Smith. Fsl. *NeuroImage*, 62(2):782 – 790, 2012. 10, 24

[27] J.T. Ratnanather, P.E. Barta, Honeycutt.N.A., N. Lee, N.G. Morris, A.C. Dziorny, M.K. Hurdal, G.D. Pearlson, and M.I. Miller. Dynamic programming generation of boundaries of local coordinatized submanifolds in the neocortex: application to the planum temporale. *NeuroImage*, 20(1):359–377, 2003. 10, 11

[28] Mark Jenkinson, Peter Bannister, Michael Brady, and Stephen Smith. Improved optimization for the robust and accurate linear registration and motion correction of brain images. *NeuroImage*, 17(2):825 – 841, 2002. 10

[29] Jidan Zhong, Desiree Yee Ling Phua, and Anqi Qiu. Quantitative evaluation of lddmm, freesurfer, and caret for cortical surface mapping. *NeuroImage*, 52(1):131 – 141, 2010. 11, 12, 17

[30] Dimitrios Pantazisa, Anand Joshi, and Richard M. Leahya. Comparison of landmark-based and automatic methods for cortical surface registration. *NeuroImage*, 49:2479–2493, 2010. 12, 15, 16

[31] M. P. Dubuisson and A. K. Jain. A modified hausdorff distance for object matching. *Proceedings of the 12th IAPR International Conference on Computer Vision and Image Processing*, 1:566–568, 1994. 15

[32] Lee R. Dice. Measures of the amount of ecologic association between species. *Ecology*, 26:297–302, 1945. 17

[33] Daniel S. Marcus, Tracy H. Wang, Jamie Parker, John G. Csernansky, John C. Morris, and Randy L. Buckner. Open access series of imaging studies (oasis): Cross-sectional mri data in young, middle aged, nondemented, and demented older adults. *Journal of Cognitive Neuroscience*, 19:1498–1507, 2007. 24

[34] L. Pantoni. *Cerebrovasc Dis*, 13 Suppl 2:7–10, 2002. 47

[35] V. G. Young, G. M. Halliday, and J. J. Kril. Neuropathologic correlates of white matter hyperintensities. *Neurology*, 71:804–11, 2008. 47

[36] O. Carmichael, C. Schwarz, D. Drucker, E. Fletcher, D. Harvey, L. Beckett, Jr. Jack, C. R., M. Weiner, and C. DeCarli. Longitudinal changes in white matter disease and cognition in the first year of the alzheimer disease neuroimaging initiative. *Arch Neurol*, 67:1370–8, 2010. 47

[37] J. He, A. M. Iosif, D. Y. Lee, O. Martinez, S. Chu, O. Carmichael, J. A. Mortimer, Q. Zhao, D. Ding, Q. Guo, D. Galasko, D. P. Salmon, Q. Dai, Y. Wu, R. C. Petersen, Z. Hong, A. R. Borenstein, and C. DeCarli. Brain structure and cerebrovascular risk in cognitively impaired patients: Shanghai community brain health initiative-pilot phase. *Arch Neurol*, 67:1231–7, 2010. 47

[38] S. Debette and H. S. Markus. The clinical importance of white matter hyperintensities on brain magnetic resonance imaging: systematic review and meta-analysis. *BMJ*, 341:c3666, 2010. 47

Declaration

I herewith declare that I have produced this paper without the prohibited assistance of third parties and without making use of aids other than those specified; notions taken over directly or indirectly from other sources have been identified as such. This paper has not previously been presented in identical or similar form to any other Singapore or foreign examination board.

The thesis work was conducted from Jan 2009 to Dec 2012 under the supervision of PI at Computational Functional Anatomy Lab in NUS.

Singapore,